Crystal and Magnetic Structure of the System $Li_{0.5+0.5x}Fe_{2.5-1.5x}Ti_xO_4$ ($x = 0.16$, 0.44, and 0.72)

María Angeles Arillo,[a] Gabriel Cuello,[b] María Luisa López,*[a] Carlos Pico,[a] and María Luisa Veiga[a]

This paper is dedicated in memoriam of Professor Antonio Jerez

Abstract: The influence of thermal treatment on the structure of lithium titanium ferrite spinels of general formula $Li_{0.5+0.5x}Fe_{2.5-1.5x}Ti_xO_4$ ($x = 0.16$, 0.44, and 0.72) has been studied by X-ray and neutron diffraction and analysed by the Rietveld method. The results allow us to conclude the presence of an ordered phase (space group $P4_332$) at room temperature for the sample with $x = 0.16$; this phase does not appear for the remaining compositions. The magnetic properties evidence a ferrimagnetic ordering in the structures when a random cation distribution (space group $Fd3m$) is obtained. An exhaustive study carried out by neutron diffraction measurements on these samples shows a different behaviour when the titanium content is increased, concluding that the lower substituted phase ($x = 0.16$) exhibits a Néel's collinear ferrimagnetic structure, with the higher substituted structures being non-collinear ($x = 0.44$ and 0.72).

Keywords: lithium titanium ferrites · magnetic properties · neutron diffraction · spinel phases

Introduction

Complex oxides derived from the spinel-type structure, AB_2O_4, are well-known magnetic materials, and ferrimagnetism is observed in Fe_3O_4 and many spinel ferrites that are used as thermistor materials. Certain oxides with two or more interacting antiferromagnetic sublattices that are canted at an angle leave a net magnetization and are called canted antiferromagnets. In general, ferrites possess high values of magnetization, because of imbalanced site magnetic moments along with high values of resistivity, low dielectric loss and high Néel temperatures. These properties have made them versatile materials for various technological applications; for example, lithium ferrite materials have dominated in the field of microwave devices, especially as replacements for garnets due to their lower cost, and some derivatives are promising candidates for high-frequency applications. It is worth noting that the crystallographic, electrical and magnetic behaviour of ferrites depend strongly upon stoichiometry as well as processing parameters such as temperature, atmosphere and pressure, mainly because affect the distribution of cations among the available tetrahedral (A) and octahedral (B) sites in the spinel lattice. Control over cation distribution provides a means of developing the desired physical properties for their technological use in industry.

Materials of general formula $Li_{0.5+0.5x}Fe_{2.5-1.5x}Ti_xO_4$ with spinel-related structures have order–disorder phase transitions that are mainly governed by the composition and the temperature. These transitions are accompanied by noticeable variations in the magnetic behaviour and a many studies on this system have been reported in the literature,[1–8] owing to their high transition temperature from ferromagnetic to paramagnetic, as occurs in the parent phase, $Li_{0.5}Fe_{2.5}O_4$, for which the transition temperature is as high as 958 K.[9–11] Though much research has been carried out about the physical properties of these derivatives and the main features of their structure and relations are now well known, there are still some controversies, especially over the composition range at which structural changes occur, and over the magnetic structure and the effect of nonmagnetic and magnetic cation substitution on various properties of lithium ferrites.[1,12–13]

The first member of this solid solution, $Li_{0.5}Fe_{2.5}O_4$ (that is, with $x = 0$) is an inverse spinel that can be formulated as $(Fe^{3+})_A[Li_{0.5}Fe_{1.5}]_BO_4$. It crystallizes in the space group $P4_332$ and has a cation ordering of 1:3-type in the octahedral sublattice[9] (being located Li^+ in 4b and Fe^{3+} in 12d sites), and the different charge of cations seem to be the responsible

[a] Prof. Dr. M. A. Arillo, Prof. Dr. M. L. López, Prof. Dr. C. Pico, Prof. Dr. M. L. Veiga
Departamento de Química Inorgánica I
Facultad de Ciencias Químicas
Universidad Complutense de Madrid
Avda. Complutense s/n, 28040 Madrid (Spain)
Fax number: (+34) 913-944-352
E-mail: marisal@quim.ucm.es

[b] Dr. G. Cuello
Institut Max von Laue-Paul Langevin (ILL)
38042 Grenoble Cedex 9 (France)

 DOI: 10.1002/chem.200400310

for this ordering. Moreover, order–disorder phase transitions at $T = 1008$–1023 K were reported for this compound.[10]

It is not yet clear in which compositional range the ordered and disordered transition occurs for the $Li_{0.5+0.5x}Fe_{2.5-1.5x}Ti_xO_4$ derivatives. Previous studies by X-ray diffraction were first reported by Blasse[1] and described these phases as cation-ordered for $x \leqq 0.33$ and disordered for $0.55 \leq x \leq 1.11$, with again an ordered distribution for higher degrees of substitution, $1.11 \leq x \leq 1.66$. This range of composition was confirmed by Schaner,[2] although Yousif[4] proposed that this system shows the 1:3 ordering for $x < 0.7$. In addition, other authors[1–5] have reported detailed studies using magnetization and Mössbauer spectroscopy for this system in the range $0 \leq x \leq 0.7$, in agreement with the cation distribution proposed by Blasse[1] and White.[6] Nevertheless no systematic structural studies have been carried out until now in the whole range of composition and the above techniques were used in order to propose non-collinear magnetic models when the Ti^{4+} content increases.

This current work is devoted to the analysis of the relationship between crystal structure and chemical composition in the system $Li_{0.5+0.5x}Fe_{2.5-1.5x}Ti_xO_4$, as well as the influence of the applied thermal treatments, by X-ray and neutron diffraction. The materials chosen have the compositions $Li_{0.58}Fe_{2.26}Ti_{0.16}O_4$, $Li_{0.72}Fe_{1.84}Ti_{0.44}O_4$ and $Li_{0.86}Fe_{1.42}Ti_{0.72}O_4$, corresponding to the values $x = 0.16$, 0.44 and 0.72, respectively. Another aim was to establish the magnetic structures by means of neutron diffraction data and to study the magnetic behaviour of the phases whose variations are induced by the actual cation distribution.

Results and Discussion

The samples of the system $Li_{0.5+0.5x}Fe_{2.5-1.5x}Ti_xO_4$ for $x = 0.16$, 0.44 and 0.72 were obtained following the experimental details given in Experimental Section by slow cooling (SC) and rapid quenching (Q) from 973 K to room temperature. These compositions are intermediate between the limits of substitution, $Li_{0.5}Fe_{2.5}O_4$ ($x = 0$) and $LiFeTiO_4$ ($x = 1$), previously described in the literature.[7,14] The main structural difference between these phases is the transition from the space group $P4_332$ to $Fd3m$, respectively.

The XRD patterns of the isolated compounds confirmed the formation of highly crystalline spinel monophases, in which some interesting differences arose. The structural refinements were made taking the above compounds, $Li_{0.5}Fe_{2.5}O_4$ and $LiFeTiO_4$, as starting models for the ordered and disordered phases, respectively.

Structural analysis by X-ray diffraction(XRD): The XRD patterns obtained at room temperature for the sample $x = 0.16$ SC (Figure 1a) show some representative reflections indexed as (110), (210) and (211), forbidden in the more conventional spinel space group $Fd3m$, that suggests the formation of a superstructure similar to this observed in the parent phase, $Li_{0.5}Fe_{2.5}O_4$. Thus, all the reflections have been adequately refined in the same $P4_332$ space group. By contrast, in the sample $x = 0.16$ Q all the observed reflections (Figure 1b) can be indexed in the $Fd3m$ space group; this implies a disordered distribution of cations at the octahedral sites. This structural change appears as a consequence of the cation ordering at the octahedral sites that is favoured by the cooling conditions.

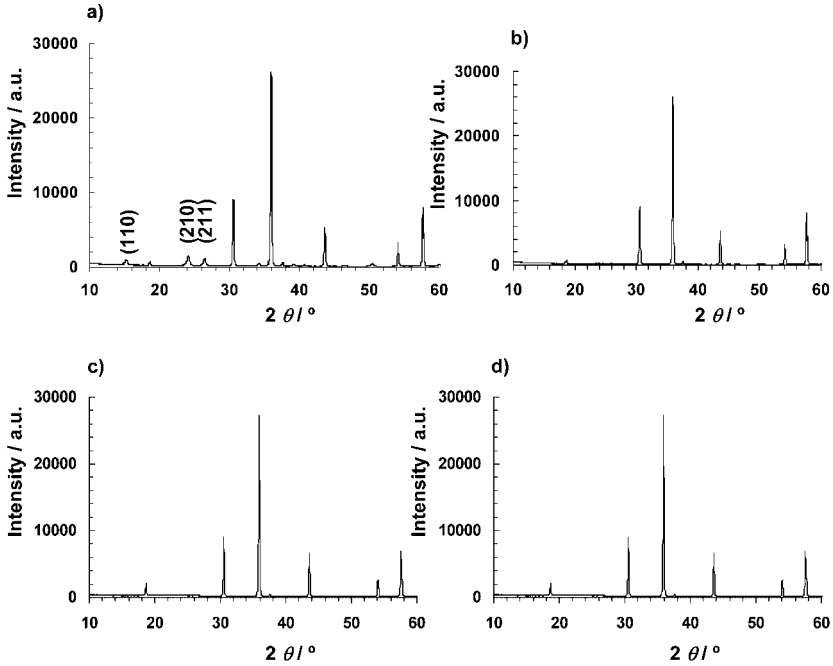

Figure 1. XRD patterns of the samples: a) $x = 0.16$ slow cooling (SC), b) $x = 0.16$ quenching (Q), c) $x = 0.44$ (SC) and d) $x = 0.44$ (Q).

These structural differences are not apparent in the samples $x = 0.44$ SC (Figure 1c) and Q (Figure 1d) and in the $x = 0.72$ SC and Q ones (not depicted), for which the respective XRD patterns were satisfactorily fitted using the $Fd3m$ space group in both cases. Therefore, only in the lower substituted phase does an order–disorder transition take place at temperatures below 973 K; this does not appear to be the case for the remaining compositions, showing that the cooling method has no influence on the cation occupancy for compositions $0.44 \leq x \leq 1.0$.

The structural model for the cation distribution in the ordered phase ($x = 0.16$ SC) is based on site preferences for cations in the spinel structure. Bearing in mind the usual

factors affecting the cation distribution, Li^+ and Fe^{3+} have no preference and could occupy each of three different cation sites,[7,8] but the Ti^{4+} ions preferably are located on the six-coordinate sites. Crystallographic data obtained in the structural refinement are given in Table 1 for $x=$ 0.16 SC; these data are compared the parent spinel $Li_{0.5}Fe_{2.5}O_4$. The refined values of occupancies for this sample lead to the following ordered distribution, in which cations occupy tetrahedral 8c and octahedral 4b and 12d sites and oxygen ions are placed in the 8c and 24e ones: $(Li_{0.05}Fe_{0.95})_{8c}[(Li_{0.37}Ti_{0.13})_{4b}(Li_{0.16}Fe_{1.31}Ti_{0.03})_{12d}]$.

Table 1. Structural parameters obtained from the Rietveld refinement from space group $P4_332$ of powder X-ray diffraction patterns for ordered compound.

		$Li_{0.5}Fe_{2.5}O_4$[a]	$Li_{0.58}Fe_{2.26}Ti_{0.16}O_4$ ($x=0.16$)
a [Å]		8.314(3)	8.335(3)
tetrahedral	8c		
sites	$x=y=z$	−0.0023	−0.0014(5)
	N[b] (Li/Fe)	0/1	0.05/0.95
octahedral	4b		
sites	$x=y=z$	5/8	5/8
	N[b] (Li/Fe)	1/0	0.37/0.13
	12d		
	x	1/8	1/8
	y	0.3674(1)	0.371(1)
	z	$^1/_4-y$	$^1/_4-y$
	N[b] (Li/Fe/Ti)	0/1/0	0.16/1.31/0.03
	8c		
	$x=y=z$	0.3853(3)	0.385(2)
	24e		
	x	0.1166(3)	0.118(3)
	y	0.1284(3)	0.125(2)
	z	0.3853(3)	0.381(2)

Bond lengths

		$Li_{0.5}Fe_{2.5}O_4$[a]	$Li_{0.58}Fe_{2.26}Ti_{0.16}O_4$
tetrahedral	M(8c)−O1	1.878×3	1.878×3
	M(8c)−O21	1.915	1.926
mean distances		1.887	1.890
octahedral 4b	M(4b)−O2	2.106×6	2.081(2)×6
octahedral 12d	M(12d)−O1	1.951×2	1.995(2)×2
	M(12d)−O2	1.999×2	2.032(3)×2
		2.058×2	2.036(2)×2
mean distances		2.003	2.021

[a] From reference [10]. [b] N = occupation.

From this distribution the cationic charge is balanced in nearly equal proportions between octahedral (overall charge 5.1+) and tetrahedral (charge 2.9+) coordinated sites as in the parent phase $Li_{0.5}Fe_{2.5}O_4$ (charge 5.0+ and 3.0+, respectively). On the other hand, the 1:3 cation ordering found in both phases is related to the high charge difference between cations located on 4b and 12d positions. These charges are, respectively, of 0.5+ and 4.5+ in the parent phase, according to its cation ordering $(Li_{0.5})_{4b}(Fe_{2.5})_{12d}$, and 0.9+ and 4.2+ in the $x=0.16$ sample. Thus, the charge difference between octahedral sites diminishes somewhat by substitution of iron by titanium. In consequence, the increasing titanium content in the 4b sites, concomitant with higher x values, reduces the effect of charges and the structure progressively tends to a random distribution of cations.

On the other hand, in ordered spinels the cations in 4b sites have six equidistant oxygen ions, whereas tetrahedrally (8c) and octahedrally (12d) coordinated cations have nearest oxygen neighbours at different distances, 3+1 and 2+2+2, respectively. These features are also evidenced in our case ($x=0.16$ SC, see Table 1). Bearing in mind that 4b octahedral sites are larger than 12d ones, the cation ordering seems to be also favoured by their size difference in octahedral coordination; this is also observed in the parent compound ($r_{Li}(VI)=0.74$ Å, $r_{Fe}(VI)=0.645$ Å). The introduction of Ti^{4+} provokes a partial displacement of Li^+ ions that migrate from 4b sites to 12d ones, causing a visible decrease of mean bond distances in the 4b octahedra and an increase of mean bond distances in the 12d octahedra. Taking into account that the Ti^{4+} ion has greater charge and smaller ionic radius ($r_{Ti}(VI)=0.605$ Å) than Li^+, the introduction of that ion in 4b positions produces a compensation of both factors, size and charge. From these arguments, the progressive introduction of Ti^{4+} ions should give a more disordered cation distribution and, as stated above, from the composition $x=$ 0.44 all cations are at random in octahedral sites.

Effectively, Figure 2 shows the mean interatomic distances in 4b and 12d octahedral sites versus the degree of substitution (x) for the title compositions and others previously reported by us.[7,8] The observed variation agrees with the above assumptions, indicating that M−O mean distances become progressively closer from the parent compound ($x=$ 0) to $x=0.44$, at which there is a change to space group $Fd3m$ that is preserved towards the upper limit of substitution, $x=1$.

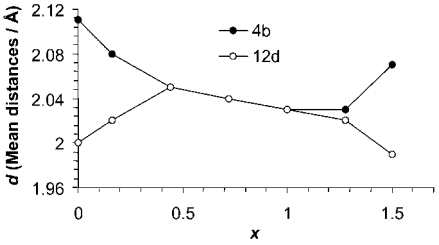

Figure 2. Mean distances versus composition for $Li_{0.5+0.5x}Fe_{2.5-1.5x}Ti_xO_4$.

For this latter phase ($LiFeTiO_4$), the actual cation distribution between tetrahedral and octahedral sites is $(Li_{0.47}Fe_{0.53})_A(Li_{0.53}Fe_{0.47}Ti)_B$. Although from this distribution an ordered structure could be favoured, we have never found such an ordering in octahedral sites.[7] For higher values of x the structure is described again in the space group $P4_332$ and the Ti^{4+} ions progressively migrate from 4b to 12d sites until $x=1.50$, whereby all Ti^{4+} ions are exclusively located on the 12d positions. Cation migration leads to an increase in the ordering from partial ($x=1.28$) to full ($x=1.50$) and, in consequence, larger differences in mean distances between 4b and 12d octahedral sites appear.

Therefore, an interesting conclusion of this structural study is that the different location of Ti^{4+} on two octahedral

sites, interpreted by the above statements of charge and composition, is the main reason for the order–disorder phenomena observed in this system. Similar results were found for other solid solutions with spinel structure.[15]

Magnetic behaviour: Magnetic susceptibility measurements were carried out on the title samples. The results obtained for quenched and slowly cooled specimens were similar in both cases and the following discussion is devoted to the Q samples.

Figure 3 shows the temperature dependence of the magnetic susceptibility, $\chi(T)$, in the temperature range between

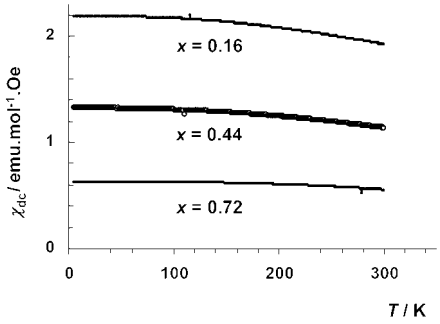

Figure 3. Variation of the dc magnetic susceptibility at 5 kOe with temperature for $x=0.16$, 0.44 and 0.72.

2 and 300 K measured at a field of 5 kOe. All the samples exhibited a slight increase of the magnetic susceptibility when temperature decreases, and no Curie–Weiss behaviour was observed over the whole range measured. The absence of a linear behaviour in the dc reciprocal susceptibility (not depicted) suggests that the transition to a paramagnetic state is to be expected for a critical temperature above 300 K.

The field dependence of magnetization, $M(H)$, measured at different temperatures up to a maximum field of 50 kOe is depicted in Figure 4. The appearance of anhysteric cycles that saturate from 2 to 50 kOe is characteristic of ferrimagnetic behaviour. According to the two-sublattice collinear spin model of ferrimagnetism by Néel,[16] the net magnetization (M) is given by the difference in magnetization between the two sublattices: $M=M_B-M_A$, where M_B and M_A are the B (octahedral) and A (tetrahedral) site magnetic moments, in μ_B.

Taking into account that the magnetic moment of Fe^{3+} ions is close to 5 μ_B and the net magnetic moments obtained by magnetization measurements at 2 K were 2.15 μ_B, 1.40 μ_B and 0.60 μ_B for $x=0.16$, 0.44 and 0.72, respectively, one can calculate the actual occupation of paramagnetic cations. Assuming a collinear magnetic model, the cation distribution in our compounds can be obtained from the following expressions: $M=n_B\mu_B(Fe^{3+})-n_A\mu_B(Fe^{3+})$ (i.e., $2.5-1.5x=n_B+n_A$) in which n_B and n_A stands for the tetrahedral and octahedral occupations, respectively. Bearing in mind that titanium cations are always occupying octahedral sites, the cation distribution for the title compounds are: $(Li_{0.09}Fe_{0.91})_A(Li_{0.49}Fe_{1.35}Ti_{0.16})_B$ (for $x=0.16$), $(Li_{0.22}Fe_{0.78})_A(Li_{0.50}Fe_{1.06}Ti_{0.44})_B$ (for $x=0.44$) and $(Li_{0.35}Fe_{0.65})_A(Li_{0.51}Fe_{0.77}Ti_{0.72})_B$ (for $x=0.72$).

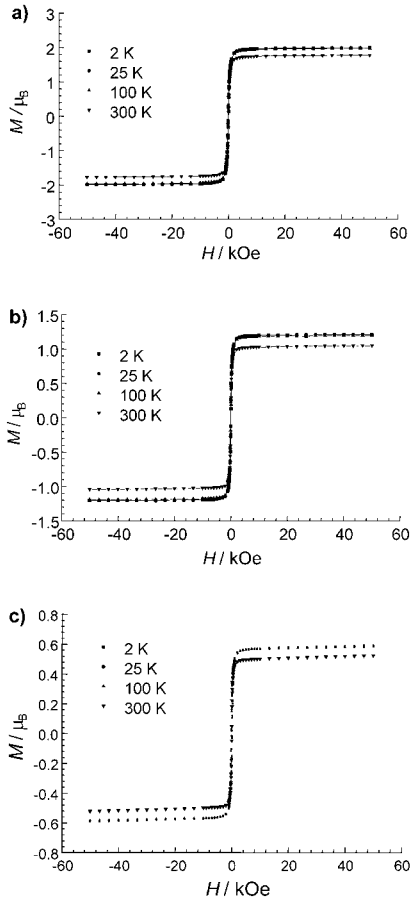

Figure 4. Magnetization versus magnetic field for a) $x=0.16$, b) $x=0.44$ and c) $x=0.72$ at different temperatures.

These results show that the lithium content in octahedral sites remains nearly constant, whereas the iron content in them sharply decreases as x increases.

Structural analysis by neutron diffraction at 973 K: The magnetic properties of a spinel complex oxide, AB_2O_4, depend strongly on how the cations are distributed over the A and B sites of the crystal lattice. Therefore, for a correct determination of the magnetic structure it is indispensable to obtain the exact distribution of the cations among the two kinds of sites in samples of good quality. To avoid the ambiguity resulting from the magnetic contribution to the Bragg intensities in determining the proper distribution of the different cations, it is essential to obtain neutron diffraction patterns that contain the nuclear contribution only. For these purposes, neutron diffraction (ND) patterns for the samples under study were taken at 973 K and the profiles were analysed by using the program Fullprof[17] and the Rietveld[18] method.

Our samples exhibit the crystallographic symmetry defined by the space group *Fd3m* and in the data refinement process this space group was used to generate the calculated profiles. The occupation number of cations at A and B sites and other structural parameters, previously obtained by

XRD at room temperature and confirmed by ND at 973 K in the paramagnetic phase, were used for the analysis of the high-resolution patterns. As stated above, ND data at 973 K only show the reflections due to a random distribution of cations without superstructure extra reflections. Figure 5

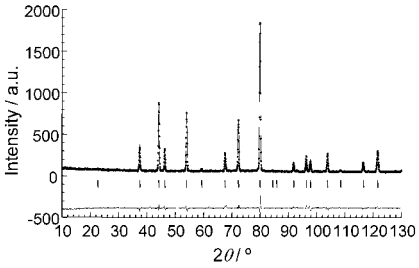

Figure 5. Observed, calculated and difference NDP (D1A) profiles of the samples $x=0.16$ at 973 K. Vertical marks correspond to the position of the allowed reflections for the space group *Fd*3*m*.

shows the fitting of experimental ND pattern corresponding to the $x=0.16$ sample and the differences between the observed and calculated profiles. This pattern is similar to those of the remaining compositions and clearly shows the change in symmetry with respect to the ordered phase of the same composition commented on before.

A summary of the structural parameters and the most representative interatomic bond lengths obtained in the refinement are given in Table 2. By comparing the cation distribution deduced from magnetization measurements and from ND, one can verify that both results are nearly identical for the $x=0.16$, and for the $x=0.44$ and 0.72 samples there are only slight differences which can be explained by the magnetic structure determination.

Table 2. Lattice parameters, *R* factors and structural parameters obtained from the Rietveld refinement of powder neutron diffraction patterns for $Li_{0.58}Fe_{2.26}Ti_{0.16}O_4$, $Li_{0.72}Fe_{1.84}Ti_{0.44}O_4$ and $Li_{0.86}Fe_{1.42}Ti_{0.72}O_4$ at 973 K.

	$x=0.16$	$x=0.44$	$x=0.72$
a [Å]	8.4027(1)	8.4140(6)	8.4273(4)
space group	*Fd*3*m*	*Fd*3*m*	*Fd*3*m*
Z	8	8	8
R_B [%]	4.78	5.10	3.58
R_P [%]	5.86	6.32	5.80
R_{WP} [%]	7.58	8.89	7.53
8*a*			
$x=y=z$	1/8	1/8	1/8
N[a](Li/Fe)	0.09/0.91	0.23/0.77	0.36/0.64
16d			
$x=y=z$	1/2	1/2	1/2
N[a](Li/Fe/Ti)	0.49/1.35/0.16	0.49/1.07/0.44	0.51/0.78/0.72
32e			
$x=y=z$	0.2564(3)	0.2567(3)	0.2587(2)
	Bond lengths		
	$x=0.16$	$x=0.44$	$x=0.72$
M(8*a*)–O	1.913(4)(×4)	1.919(8)×x4)	1.958(7)(×4)
M(16d)–O	2.047(8)(×6)	2.048(5)(×6)	2.063(3)(×6)

[a] N = occupation.

Magnetic structure: Figure 6 shows ND patterns collected at 973 and 300 K for the $x=0.16$ and 0.44 phases; that of $x=0.72$ is similar to the latter. The measurements at 300 K were obtained after cooling the samples in the furnace from

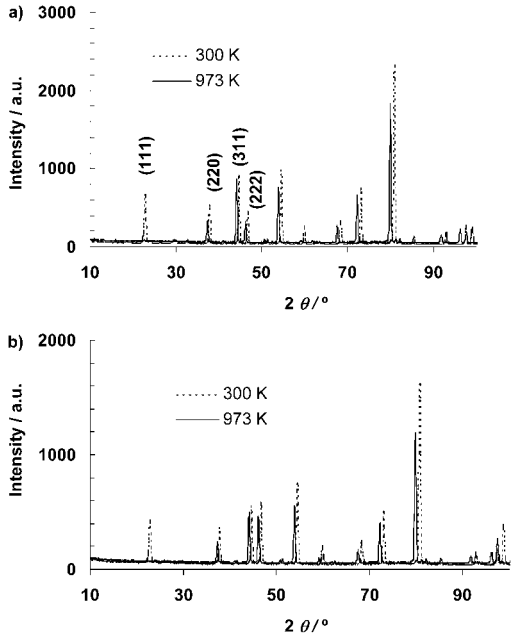

Figure 6. Observed neutron powder diffraction pattern at 300 K and 973 K for a) $x=0.16$ and b) $x=0.44$.

973 K. By comparing both patterns, noticeable changes are observed in certain Bragg reflections. At 973 K the diffraction peaks are characteristic of only the nuclear scattering, whereas at 300 K the (111), (220), (311) and (222) reflections increase in intensity with respect to the 973 K patterns. Thus, the observed variations should be due to magnetic interactions, according to the above magnetic measurements. All magnetic peaks can be indexed with a propagation vector $\boldsymbol{k}=(000)$, referring to the high temperature unit cell, indicating that both the magnetic and nuclear cells are similar.

Moreover, in the thermodiffractograms collected between 2 and 300 K for $x=0.16$ (Figure 7a) revealed the presence of some additional peaks at low angles, indexed as (110), (210) and (211), characteristic of the ordered phase Therefore, the sample $x=0.16$ exhibited a minor phase with cation ordering on the octahedral sites, resulting in a superstructure that could be refined in the $P4_332$ space group.

The Bragg peaks remain sharp throughout in this temperature range, heralding the presence of long-range magnetic ordering (LRO). An interesting feature at this respect is the appearance of the (200) reflection in the patterns of the $x=0.44$ and 0.72 samples (Figure 7b and Figure 7c), which is absent in that of $x=0.16$, and could be related to a different spin orientation.

Since these spinel ferrites can be considered as ionic compounds, in which the only paramagnetic cation is Fe^{3+} and recalling the observed cation distribution, it is possible to estimate the sublattice moments at saturation, assuming a col-

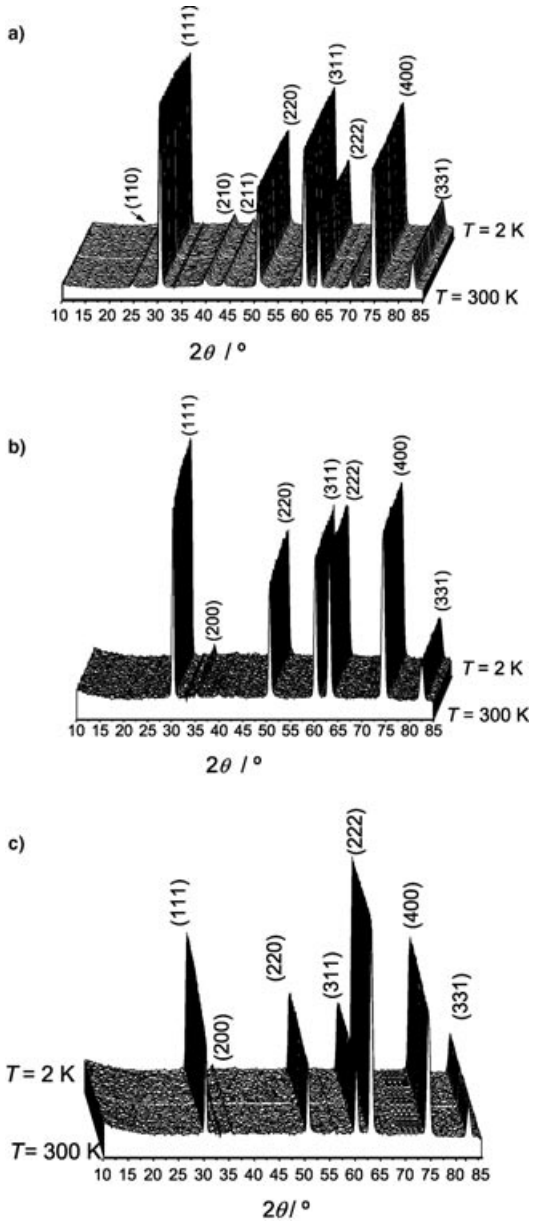

Figure 7. Thermal evolution of NDP collected at a wavelength $\lambda = 2.522$ Å in the temperature range 2–300 K for a) $x = 0.16$, b) $x = 0.44$ and c) $x = 0.72$ samples.

linear ordering. If the magnetic ions are all in such a Néel ordering, then one expects the site moments deduced from the normal Bragg reflections are to be close to the estimated free-ion moments, because in such a situation the moments of the magnetic ions will be fully aligned along the longitudinal direction (i. e., along the axis of broken symmetry). However, if the magnetic ordering is noncollinear, then the ordered site moments deduced will correspond only to the longitudinal components, since the transverse components do not contribute to the intensities of the normal Bragg reflections. The spatial ordering of the transverse components of magnetic moments at the B sublattice can give rise to (200) superlattice reflection,[19,20] which is purely magnetic in nature and is responsible of the existence of LRO. From the low angle neutron diffraction patterns shown in Figure 7, it is clear that such a (200) reflection is present for the $x = 0.44$ and 0.72 samples.

Rietveld refinements of ND patterns carried out at 300 K for all samples were tried on the basis of collinear and noncollinear models. Figure 8 shows the fitting results that contain both nuclear and magnetic contributions. The site occupancies deduced from the analysis of the high-temperature ND data were kept fixed and all the other parameters were varied during the refinement. The best fits were obtained assuming: 1) a multiphase refinement using both the ordered ($P4_332$) and disordered ($Fd3m$) structures [21,22] with a collinear model, for $x = 0.16$; and 2) a refinement using the $Fd3m$ space group with a noncollinear model, for $x = 0.44$ and 0.72. The discrepancy factors were $R_B = 4.15$ and $R_M = 3.89$ for $x = 0.16$, $R_B = 3.95$ and $R_M = 4.90$ for $x = 0.44$, and $R_B = 5.63$ and $R_M = 6.74$ for $x = 0.72$. These R factors are indicative that the structural and magnetic models are adequate for all the samples.

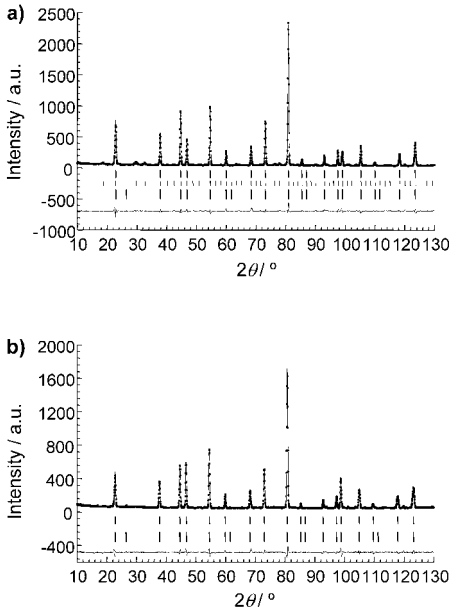

Figure 8. Observed (circles) and calculated (continuous line) NPD intensity profiles and at the bottom the difference plot is shown. The short vertical lines indicate the angular position of the allowed Bragg reflections. for a) $x = 0.16$ space group $Fd3m$ (upper vertical marks), $P4_332$ (middle vertical marks) and magnetic contribution (lower vertical marks)and b) $x = 0.44$ space group $Fd3m$ (upper vertical marks), and magnetic contributions (lower vertical marks).

The calculated sublattice magnetic moments and total magnetic moment ($M_T = M_B - M_A$) as well as the expected magnetic moments, taking into account the cation occupancies and considering the spin only moment for Fe^{3+} (5 μ_B), are shown in Table 3. By comparing the magnetic moments obtained from magnetization measurements at low temperature (2 K) and those obtained from structural results (denoted as "expected" in Table 3), we can conclude that both sets of data are similar for $x = 0.16$, but differs for $x = 0.44$ and 0.72. Therefore, in $x = 0.16$ we assume a collinear model, whereas in the remaining phases a noncollinear model must be considered. On the other hand, at room temperature

Table 3. Magnetic moments in μ_B for for $Li_{0.58}Fe_{2.26}Ti_{0.16}O_4$, $Li_{0.72}Fe_{1.84}Ti_{0.44}O_4$ and $Li_{0.86}Fe_{1.42}Ti_{0.72}O_4$.

	$x=0.16$	$x=0.44$	$x=0.72$
M_A(expected)	4.55	3.70	3.20
M_B (expected)	6.75	5.50	3.90
M_T (expected)	2.20	1.50[a]	0.70[a]
M_T (cycle 2k)	2.15	1.4	0.60
M_T (cycle 300 K)	1.8	1.0	0.55
M_A (ND 300 K)	3.42	2.44	2.62
M_B (ND 300 K)	5.36	y 0.78	y 0.35
		z 3.47	z 2.06
M_T (ND 300 K)	1.94	1.03	0.56

[a] A collineal model is supposed.

these different models are still operative and there is a good agreement between the deduced magnetic moments from magnetization and ND.

The above conclusions are confirmed by the neutron thermodiffractograms carried out in the range 2–300 K (for details see the Experimental Section). The temperature variation of the sublattice and net magnetic moments obtained from the data refinement are shown in Figure 9. From the cation distributions listed in Table 2, the sublattice moments for the compositions of present system have been estimated. In the sample $x=0.16$, in which the moments of all the magnetic ions are ordered in the longitudinal direction, the observed sublattice moments are very close to those expected. However, the noncollinear model proposed for $x=0.44$ and 0.72 shows the loss of the ordered moments at the B sites, in good agreement with the results obtained in the $M(H)$ curves.

The collinear and noncollinear models are schematically depicted in Figure 10. In the collinear ordering (Figure 10a),

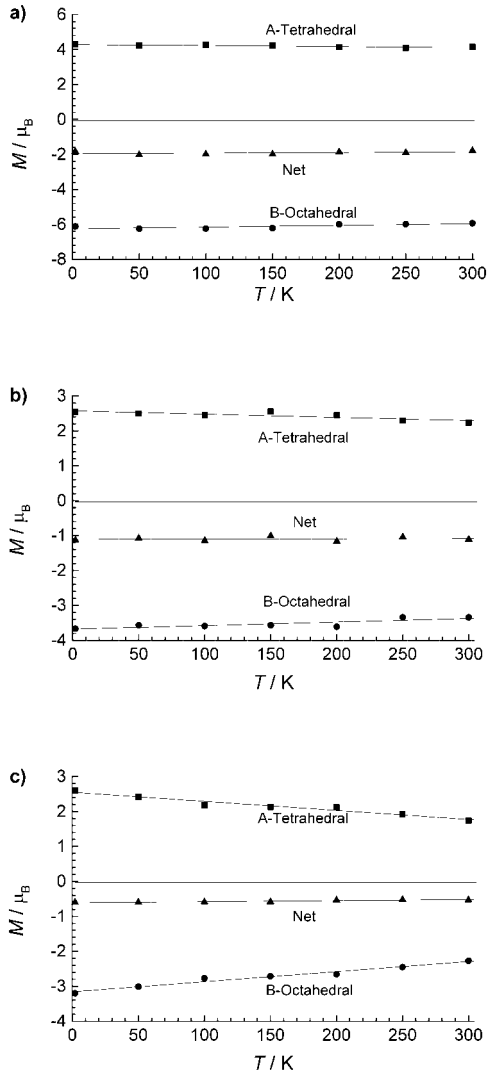

Figure 9. Variation of the sublattice and the net magnetic moments with temperature a) $x=0.16$, b) $x=0.44$ and c) $x=0.72$.

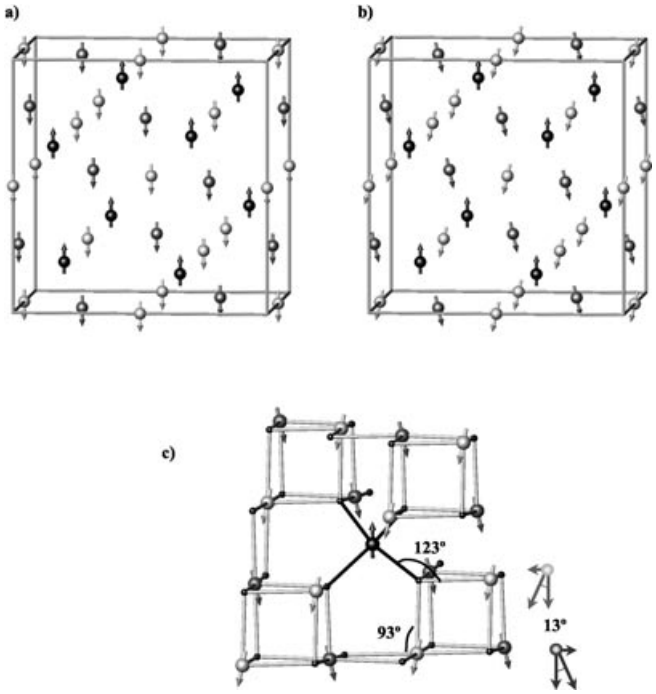

Figure 10. Projection of the magnetic lattice of tetrahedral and octahedral sites, showing spin model: a) collinear ordering, b) noncollinear ordering and c) exchange mechanism between A and B sublattices.

the A and B sublattice spins are oriented along the c axis and are mutually antiparallel. For the noncollinear model (Figure 10b), the tetrahedral A cations maintain their ferromagnetic ordering, whereas the octahedral B ones show an internal canting angle close to 13° with respect to z axis (Figure 10c). This canting is provoked by a mutual antiferromagnetic alignment in the transversal component, along the y axis.

In general, the indirect-exchange mechanisms that produce spontaneous magnetization are at an optimum if two interacting cations are located on opposite sites of an anion (i.e., angle M-O-M close to 180°). These coupling rules are not directly applicable to spinels, because the A–anion–B angles are ~123°, and the B–anion–B angles are ~93° (Figure 10c). The importance of the relative symmetry of the cation outer-electron wave functions and near-neighbour–anion configuration was pointed out by Goodenough and Loeb[23] and later amplified by McClure[24] and Dunitz and Orgel[25] for spinel-type oxides. Tetrahedral A cations have

the triply degenerate t_2 (d_{xy}, d_{yz}, d_{zx}) orbitals pointing towards near-neighbours anions, and B-site cations have the doubly degenerate e_g (d_{z^2}, $d_{x^2-y^2}$) orbitals pointing towards near-neighbours anions; the d_{xy}, d_{yz}, and d_{zx} orbitals point towards near-neighbours B cations. In our case ($x=0.16$) the paramagnetic Fe^{3+} ions are located in both tetrahedral and octahedral sites, and the A-site t_2 orbitals and the B-site e_g orbitals are half filled, their mutual interactions being strongly antiferromagnetic, giving rise to a normal Néel coupling (A and B moments antiparallel).

In the $x=0.44$ and 0.72 sample, both sublattices A and B are magnetically more diluted, with a higher content of Li^+ in tetrahedral sites (see Table 2), and the antiferromagnetic A–B interactions are relatively weak. On the other hand, B-site t_{2g} orbitals are half-filled and direct B–B antiferromagnetic interactions are then possible. In these samples, the $Fe_{(A)}$–$Fe_{(B)}$ and the $Fe_{(B)}$–$Fe_{(B)}$ interactions must be comparable and in consequence, as Yafet and Kittel[26] have suggested, the magnetic moments between both sublattices may not be collinear as is evidenced in Figure 10b and c.

We can conclude that magnetic dilution in these spinels provokes an enhancement of direct B–B antiferromagnetic interactions and a weakness of A–B interactions giving rise to a transversal component with long-range order.

Experimental Section

Polycrystalline lithium titanium ferrite samples with the chemical formula $Li_{0.5+0.5x}Fe_{2.5-1.5x}Ti_xO_4$ ($x=0.16$, 0.44 and 0.72) were prepared by the "liquid mix" technique[27] from powdered mixtures of Li_2CO_3, Fe_2O_3 and TiO_2 (all reactants were supplied by Merck, Germany), in stoichiometric ratios. The samples were obtained by two methods: rapid quenching (Q) from temperatures above 973 K for 12 h ($x=0.16$) or on slow cooling (SC) ($x=0.44$) at 973 K for a day to room temperature.

Neutron powder diffraction data were performed at the Institute Laue-Langevin (Grenoble, France) at different temperatures for the samples $x=0.16$ (Q) and 0.44 (SC) on the D1A high-resolution powder diffractometer ($\lambda=1.9110$ Å). The multidetector D1B powder diffractometer ($\lambda=2.522$ Å) was used for the thermal patterns in the temperature range 2–300 K. Diffraction patterns were analysed by the Rietveld[18] method and the Fullprof program[17].

Magnetic susceptibility measurements were performed in a commercial superconducting quantum interference device magnetometer, Quantum Design Magnetic Properties Measurement System 5S, on powder samples in a temperature range from 2 K to 300 K under an applied magnetic field of 5000 Oe. The magnetic field isothermal variations up to 50 kOe were obtained with the aid of a Quantum Design Physical Properties Magnetic System, which allowed for the experimental setting of highly homogeneous magnetic field at specific temperatures.

Acknowledgement

Financial support through research Project MAT2002–01288 (CICYT, Spain) and MAT2003–06003 (CICYT, Spain) are acknowledged. One of the authors (M.A.A.) is grateful to CICYT for a Postdoctoral Fellowship. We also thank to the ILL facilities.

[1] G. Blasse, *Philips Res. Rep. Suppl.* **1964**, *3*, 96–102.
[2] S. Scharner, W. Weppner, P. Schmid-Beurmann, *J. Solid State Chem.* **1997**, *134*, 170–181.
[3] A. H. Wakif, S. A. Mazen, and S. F. Mansour, *J. Phys. D.***1993**, *26*, 2010–2014.
[4] A. A. Yousif, M. E. Elzain, S. A. Mazen, H. H. Sutherland, M. H. Abdalla and S. F. Masour, *J. Phys. Condens. Matter* **1994**, *6*, 5717–5724.
[5] S. A. Mazen, A. H. Wakif and S. F. Mansour, *J. Mater. Sci.* **1996**, *31*, 2661–2665.
[6] G. O. White, C. E. Patton, *J. Magn. Magn. Mater.* **1978**, *9*, 299–317.
[7] M. A. Arillo, M. L. López, E. Perez-Cappe, C. Pico, M. L. Veiga, *Solid State Ionics* **1998**, *107*, 307–312.
[8] M. A. Arillo, M. L. López, C. Pico, M. L. Veiga, J. Campo, J. L. Martínez, A. Santrich-Badal, *Eur. J. Inorg. Chem.* **2003**, *13*, 2397–2405.
[9] "Magnetic Properties of Ferrites": M. Guillot, *Electronic and Magnetic Properties of Metals and Ceramics* (Ed.: K. H. J. Buschow), VCH, Germany, **1994**.
[10] S. J. Marin, M. O'Keeffe, D. E. Partin, *J. Solid State Chem.* **1994**, *113*, 413–419.
[11] P. B. Braun, *Nature* **1952**, *27*, 1123.
[12] S. S. Bellad, R. B. Panja, *Mater. Chem. Phys.* **1998**, *52*, 166–169.
[13] U. N. Trivedi, K. H. Jani, K. B. Modi and H. H. Joshi, *J. Mater. Sci. Lett.* **2000**, *19*, 1271–1273.
[14] A. Tomas, P. Laruelle, J. L. Dormán and M. Nogués, *Acta Crystallogr. Sect. C* **1983**, *39*, 1617–1619.
[15] N. Jovic, B. Antic, A. Spasojevic-de Bire, V. Spasojevic, *Phys. Status Solidi A* **2003**, *198*, 18–28.
[16] K. Standly, *Oxide magnetic Materials*, Clarendon, Oxford, **1972**.
[17] J. Rodríguez Carvajal, FULLPROF, XV Congress of International Union of Crystallography, Toulouse **1990**, p. 127, **1994** (Revised version).
[18] H. M. Rietveld, *J. Appl. Crystallogr.* **1969**, *2*, 65–71.
[19] N. S. Satya Murthy, M. G. Natera, S. I. Youssef, R. J. Begum and C. M. Srivastava, *Phys. Rev.* **1969**, *181*, 969–977.
[20] R. Chakravarthy, L. Madhav Rao, S. K Paranjpe, S. K. Kulshrestha, and S. B. Roy, *Phys. Rev. B* **1991**, **43**, 6031–6036.
[21] W. Branford, M. A. Green, D. A. Neumann, *Chem. Mater.* **2002**, *14*, 1649–1656.
[22] L. Fernández-Barquín, M. V. Kuznetsov, Y. G. Morozov, Q. A. Pankhurst, I. P. Parkin, *Int. J. Inorg. Mater.* **1999**, *1*, 311–316.
[23] J. B. Goodenough, A. L. Loeb, *Phys. Rev.* **1955**, *98*, 391–393.
[24] D. S. McClure, *Phys. Chem. Solids* **1957**, *3*, 311–315.
[25] J. D. Dunitz, L. E. Orgel, *Phys. Chem. Solids* **1957**, *3*, 318–320.
[26] Y. Yafet, C. Kittel, *Phys. Rev.* **1952**, *87*, 290–295.
[27] M. Pechini, US Patent , **1967**, 3 231/328.

Received: March 30, 2004
Revised: June 22, 2004
Published online: October 8, 2004